15

Shearing deformations in beams

15.1 Introduction

Euler-Bernoulli beam theory is developed in chapter 5 based on the purely kinematic assumptions discussed in section 5.1. In particular, the cross-section of the beam is assumed to remain plane after deformation, and furthermore, this plane is assumed to remain normal to the deformed axis of the beam. This second assumption implies the vanishing of the transverse shear strains, $\gamma_{12} = 0$, and leads to the following result for a beam made from a linearly elastic, homogeneous and isotropic material

$$V_2 = \int_{\mathcal{A}} \tau_{12} \, \mathrm{d}\mathcal{A} = \int_{\mathcal{A}} G\gamma_{12} \, \mathrm{d}\mathcal{A} = 0, \tag{15.1}$$

where the second integral is the result of using the constitutive law relating shear stresses to shear strains, $\tau_{12} = G\gamma_{12}$.

On the other hand, equilibrium conditions require a non-vanishing transverse shear force, V_2, to equilibrate the distributed transverse load, $p_2(x_1)$, applied to the beam, see eq. (5.38). This apparent contradiction with eq. (15.1) can be resolved through the following reasoning: as required by equilibrium, the shear stress, τ_{12}, does not vanish, but the corresponding shear strain is vanishingly small. This implies a very large shearing modulus, $G \to \infty$, so that a vanishing shear strain $\gamma_{12} \to 0$, results in a product, $G\gamma_{12} = \tau_{12}$, that becomes a finite, non-vanishing quantity.

In view of this reasoning, the assumption "plane sections remain normal to the deformed axis of the beam," which implies the vanishing of the transverse shear strains, could be replaced by "the beam is made of a material with an infinite shear modulus." Because such a constitutive law is awkward, the transverse shear force (the stress resultant associated with the shear stress), is not evaluated from this constitutive law but from equilibrium considerations instead. In fact, the shear force is altogether eliminated from Euler-Bernoulli beam theory using equilibrium considerations, see eq. (5.39), and can be recovered from the bending moment as $V_2 = -\mathrm{d}M_3^c/\mathrm{d}x_1$, eq. (5.38).

In reality, the shear modulus is of the order of Young's modulus and for isotropic materials, $G = E/(2(1+\nu)$. To investigate the effects of the additional flexibility

of the beam introduced by shear deformation, a formulation must be developed that allows for non-vanishing transverse shear strains. In this case, the assumption "plane sections remain normal to the deformed axis of the beam" can no longer be made.

Two important questions must be addressed by this new formulation: *(1)* how do shearing deformations affect the transverse displacement of the beam, and *(2)* what is the distribution of shear stresses over the cross-section of the beam? The resulting theoretical description for shear deformable beams is generally referred to as *Timoshenko beam theory*.

15.1.1 A simplified approach

Consider a beam with a rectangular cross-section of width b and depth h subjected to a shear force, V_2. In this very simplified approach, the shear stresses are assumed to be uniformly distributed over the cross-section of the beam as depicted in fig. 15.1 which shows a differential segment along the length of a beam. The shear resultant can be calculated as

$$V_2 = \int_{\mathcal{A}} \tau_{12} \, \mathrm{d}\mathcal{A} = \tau_{12} \int_{\mathcal{A}} \mathrm{d}\mathcal{A} = \mathcal{A}\tau_{12}, \tag{15.2}$$

and hence, the shear stress is $\tau_{12} = V_2/\mathcal{A}$.

If the beam is made of a homogeneous, linearly elastic material, the transverse shear strain is also uniformly distributed over the cross- section, $\gamma_{12} = \tau_{12}/G = V_2/(G\mathcal{A})$; hence, the local shear strain, γ_{12}, can also be interpreted as a sectional shear strain. The sectional constitutive law is then

$$V_2 = G\mathcal{A}\,\gamma_{12}, \tag{15.3}$$

where $G\mathcal{A}$ is the sectional *shear stiffness*.

Figure 15.1 shows that $\mathrm{d}\bar{u}_1/\mathrm{d}x_2 = 0$, and the transverse shear strain therefore becomes $\gamma_{12} = \mathrm{d}\bar{u}_1/\mathrm{d}x_2 + \mathrm{d}\bar{u}_2/\mathrm{d}x_1 = \mathrm{d}\bar{u}_2/\mathrm{d}x_1$. Equation (15.3) now implies

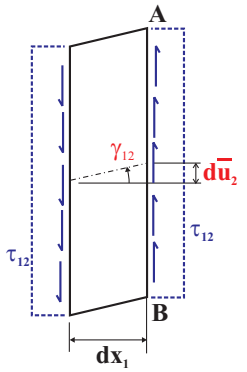

Fig. 15.1. Simplified deformation under shear.

$$\frac{\mathrm{d}\bar{u}_2}{\mathrm{d}x_1} = \frac{V_2}{G\mathcal{A}}. \tag{15.4}$$

This equation can be integrated to yield the transverse displacement field, $\bar{u}_2(x_1)$, associated with shear deformation.

Finally, the strain energy due to the shear deformation of a differential segment of the beam is

$$\mathrm{d}A = \frac{1}{2}\int_{\mathcal{A}} \tau_{12}\gamma_{12} \, \mathrm{d}\mathcal{A}\mathrm{d}x_1 = \frac{1}{2}\int_{\mathcal{A}} \frac{\tau_{12}^2}{G} \, \mathrm{d}\mathcal{A}\mathrm{d}x_1 = \frac{1}{2}\frac{\tau_{12}^2}{G}\mathcal{A} \, \mathrm{d}x_1 = \frac{1}{2}\frac{V_2^2}{G\mathcal{A}} \, \mathrm{d}x_1. \tag{15.5}$$

These developments provide a crude description of shear deformation effects in beams. The shear stress distribution is uniform over the cross-section, the sectional

shear stiffness is $G\mathcal{A}$, and the transverse displacements, $\bar{u}_2$, stemming from shear deformation can be obtained by integrating eq. (15.4).

Unfortunately, this simplified description is wrong because it violates a basic equilibrium condition. The principle of reciprocity of shear stresses, eq. (1.5), requires the shear stress, τ_{12}, to vanish at points **A** and **B**, see fig. 15.1, because the upper and lower faces of the beam are stress free. It follows that the shear stress distribution cannot possibly be uniform over the cross-section of the beam.

15.1.2 An equilibrium approach

To remedy the shortcomings of the simplified representation developed in the previous section, equilibrium conditions for the problem must be established. Figure 15.2 depicts a differential element of the beam with a rectangular cross-section of width b and depth h. Loading is applied in plane $(\bar{\imath}_2, \bar{\imath}_1)$, and consequently, stresses are uniform across the width of the section. Consider now a differential element in depth, as highlighted in fig. 15.2. Summing forces along axis $\bar{\imath}_1$ yields the following equilibrium equation

$$\frac{\mathrm{d}\sigma_1}{\mathrm{d}x_1} + \frac{\mathrm{d}\tau_{12}}{\mathrm{d}x_2} = 0. \tag{15.6}$$

This equation indicates that the distribution of shear stress through the depth of the section is related to the distribution of axial stress along the span of the beam. Consequently, simply assuming a certain shear stress distribution through the depth as is done in the previous section is unlikely to satisfy the basic equilibrium condition expressed by eq. (15.6).

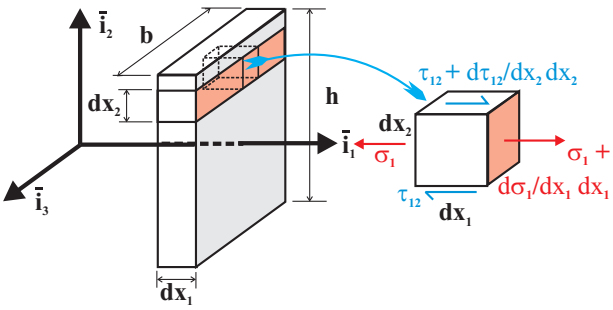

Fig. 15.2. Configuration of a differential element of the beam.

The purely kinematic Euler-Bernoulli assumptions state that the cross-section of the beam remains plane after deformation, and furthermore, this plane remains normal to the deformed axis of the beam. In the present development, the second assumption cannot be made, as it implies the vanishing of the transverse shear strains. The first assumption implies an axial displacement field in the form of eq. (5.2): $u_1(x_1, x_2, x_3) = -x_2 \Phi_3(x_1)$, where $\Phi_3(x_1)$ is the rotation of the section about axis $\bar{\imath}_3$.

For simplicity, the origin of the axis system is assumed to be located at the centroid of the section, *i.e.*, $x_{2c} = 0$. The axial strain distribution is then obtained as $\epsilon_1 = -x_2 \mathrm{d}\Phi_3/\mathrm{d}x_1$. The axial stress distribution follows from Hooke's law as $\sigma_1 = -Ex_2 \mathrm{d}\Phi_3/\mathrm{d}x_1$.

The basic equation of equilibrium, eq. (15.6), can now be used to solve for the shear stress distribution

$$\frac{\mathrm{d}\tau_{12}}{\mathrm{d}x_2} = -\frac{\mathrm{d}\sigma_1}{\mathrm{d}x_1} = Ex_2 \frac{\mathrm{d}^2\Phi_3}{\mathrm{d}x_1^2}. \tag{15.7}$$

Integration yields $\tau_{12} = Ex_2^2/2 \ \mathrm{d}^2\Phi_3/\mathrm{d}x_1^2 + c$, where c is an integration constant that can be evaluated by imposing the boundary condition, $\tau_{12}(x_2 = \pm h/2) = 0$, to find

$$\tau_{12} = \frac{1}{2} E \left(\frac{h}{2}\right)^2 \left[\left(\frac{2x_2}{h}\right)^2 - 1\right] \frac{\mathrm{d}^2\Phi_3}{\mathrm{d}x_1^2}. \tag{15.8}$$

This result is a parabolic distribution of the shear stress through the depth of the cross-section.

Next, the resultant shear force is obtained by integration of shear stress distribution over the cross-section, eq. (5.9), to find

$$\begin{aligned} V_2 &= \frac{1}{2} E \left(\frac{h}{2}\right)^2 \frac{\mathrm{d}^2\Phi_3}{\mathrm{d}x_1^2} \int_{-h/2}^{h/2} \int_{-b/2}^{b/2} \left[\left(\frac{2x_2}{h}\right)^2 - 1\right] \mathrm{d}x_2 \mathrm{d}x_3 \\ &= -\frac{1}{3} E\mathcal{A} \left(\frac{h}{2}\right)^2 \frac{\mathrm{d}^2\Phi_3}{\mathrm{d}x_1^2}, \end{aligned}$$

Finally, the sectional rotation, Φ_3, is eliminated with the help of eq. (15.8) to obtain the shear stress distribution in terms of the applied shear force,

$$\tau_{12} = \frac{3V_2}{2\mathcal{A}} \left[1 - \left(\frac{2x_2}{h}\right)^2\right]. \tag{15.9}$$

Figure 15.3 shows this parabolic shear stress distribution through the depth of the section. For reference, the uniform distribution postulated in the simplified representation is also shown in the figure. The maximum shear stress, $\tau_{\max} = 3V_2/2\mathcal{A}$, occurs at $x_2 = 0$ and is 50% higher than that obtained for the uniform distribution, $\tau_{12} = V_2/\mathcal{A}$. Clearly, the simplified representation is erroneous and grossly underestimates the maximum shear stress.

The strain energy associated with the shear deformation in a differential segment of the beam is

$$\mathrm{d}A = \frac{1}{2} \int_{\mathcal{A}} \frac{\tau_{12}^2}{G} \ \mathrm{d}\mathcal{A}\mathrm{d}x_1 = \frac{1}{2} \int_{-h/2}^{h/2} \frac{b}{G} \left(\frac{3V_2}{2\mathcal{A}}\right)^2 \left[1 - \left(\frac{2x_2}{h}\right)^2\right]^2 \mathrm{d}x_2 \mathrm{d}x_1.$$

After integration, the strain energy becomes

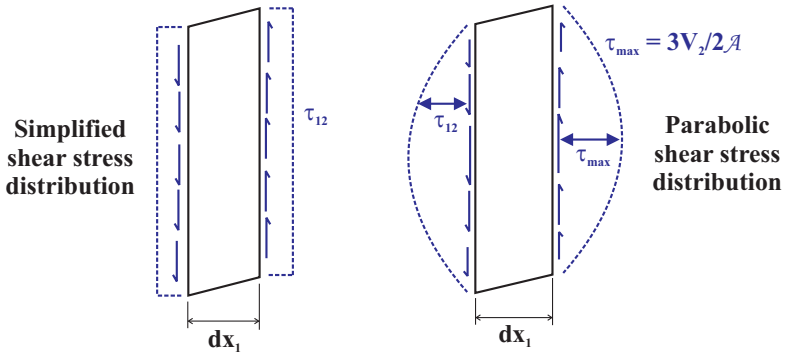

Fig. 15.3. Shear stress distribution for a rectangular section.

$$\mathrm{d}A = \frac{1}{2}\frac{V_2^2}{G\mathcal{A}}\frac{6}{5} = \frac{1}{2}\frac{V_2^2}{K_{22}}\,\mathrm{d}x_1, \tag{15.10}$$

where the sectional *shear stiffness*, K_{22}, is defined as the denominator in the expression for the strain energy in eq. (15.10). For for the rectangular cross-section,

$$K_{22} = \frac{5}{6}G\mathcal{A}. \tag{15.11}$$

This result should be contrasted with the sectional shear stiffness $K_{22} = G\mathcal{A}$ found for the simplified solution that overestimates the shear stiffness by about 20%.

The deformation of the cross-section associated with the present representation is more complex than that obtained with the simplified model. Indeed, the parabolic shear stress distribution is associated with a parabolic distribution of shear strain. The following reasoning then implies that the axial displacement field must present the "S" shape shown in the right hand side of fig. 15.4. First, the vanishing of the shear strain at points **A** and **B** implies that the initial right angle between the beam's upper or lower surfaces and the cross-section plane must remain a right angle. Second, the change in the initially right angle between the beam axis and the cross-section plane, which is a direct measure of γ_{12}, will be maximum at the midpoint ($x_2 = 0$) of the cross-section. This "S" shaped axial displacement field directly contradicts the kinematic assumption underlying the present analysis: plane sections remain plane. Hence, the present solution is inconsistent.

Equivalent shear deformation model

Although the simplified deformation shown in fig. 15.4 is incorrect, it has the advantage of conveying a very simple picture of the deformation pattern. This raises the question as to whether it is possible to make the simplified and actual representations equivalent in some sense. One approach is to find the average shear strain, γ_{ave}, in the simplified deformation that will be equivalent to the more complex shear strain distribution obtained from equilibrium analysis.

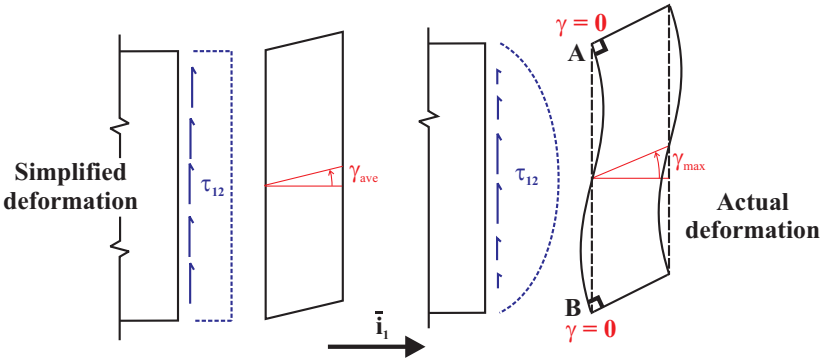

Fig. 15.4. The simplified and actual deformation configurations.

This equivalence can be obtained in an energy sense: the shear strain, γ_{ave}, can be selected so that the strain energies associated with the two deformation patterns are equal. From eqs. (15.5) and (15.10), this requires $1/2\ V_2^2/K_{22} = 1/2\ V_2\gamma_{\text{ave}}$ which can be solved for the equivalent average shear strain

$$\gamma_{\text{ave}} = \frac{V_2}{K_{22}}. \tag{15.12}$$

For the simplified model the strain-displacement relations reduces to $\gamma_{\text{ave}} = \mathrm{d}\bar{u}_2/\mathrm{d}x_1$, and hence,

$$\frac{\mathrm{d}\bar{u}_2}{\mathrm{d}x_1} = \frac{V_2}{K_{22}}. \tag{15.13}$$

This equation can be integrated to yield the transverse displacement field associated with shear deformation.

In summary, the following facts about shear deformation are established. The axial and shear stress distributions are related through an equilibrium condition, eq. (15.6). Assuming plane sections to remain plane, a linear distribution of axial stress is obtained for beam made of a linearly elastic, homogeneous material. The shear stress profile that is in equilibrium with this axial stress distribution can then be obtained from the equilibrium equation. A parabolic shear stress distribution, eq. (15.9), is found for a rectangular cross-section. The deformation of the section due to the parabolic variation of shear strain results in warping of the cross-section and violates the basic kinematic assumption of plane sections remaining plane. Consequently, the development presented here leads to an inconsistent and therefore approximate solution of the problem. Finally, the simplified deformation presented in the previous section, and the more realistic deformation presented here can be made equivalent in an energy sense by selecting the average sectional shear strain to be that given by eq. (15.12). The shear stiffness is found to be $K_{22} = 5/6\ G\mathcal{A}$ for a rectangular cross-section.

Example 15.1. Shear distribution in a sandwich section

Consider the cross-section of a sandwich beam depicted in fig. 15.5. Such structures are typically made of two thin faces of thickness t_f and Young's modulus E_f that are designed to carry most of the bending stresses. The faces sandwich a core of much lighter material that is often highly anisotropic. The core material usually has a very low Young's modulus in the directions parallel to the faces, a moderate Young's modulus in the direction perpendicular to the faces, and a moderate shear modulus, G_c. A reasonable assumption is that Young's modulus for the core material, E_c, is orders of magnitude smaller than that of the faces; hence, setting $E_c \approx 0$ is a very reasonable approximation.

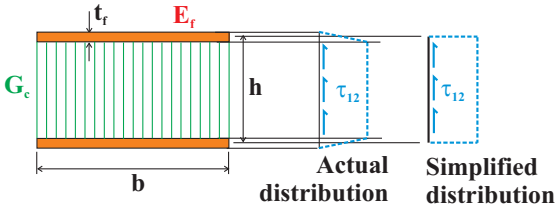

Fig. 15.5. Shear stress distribution on the cross-section of a sandwich section.

Under these assumptions, the bending stiffness of the sandwich section is due to the faces alone and is given by

$$H_{33}^c = 2\left[\frac{bt_f^3 E_f}{12} + bt_t E_f \left(\frac{h}{2}\right)^2\right] = \frac{1}{2} bt_t h^2 E_f \left[1 + \frac{1}{3}\left(\frac{t_f}{h}\right)^2\right] \tag{15.14}$$

where the first term represents the bending stiffness of the thin face with respect to its own centroid, and the second term is the transport term. The core does not significantly contribute to the bending stiffness because its intrinsic stiffness is negligible. In typical constructions, the face thickness is much smaller than the sandwich depth, *i.e.*, $t_f/h \ll 1$, and the bending stiffness reduces to

$$H_{33}^c = \frac{1}{2} bt_t h^2 E_f. \tag{15.15}$$

This results explains why sandwich structures are efficient lightweight structures in bending: the bending stiffness is proportional to the square of the sandwich depth, rather than the cube of the face thickness, while the low density core material contributes to a low overall density. In effect, the core material contributes little to the bending stiffness but keeps the two faces a distance h apart, dramatically increasing their contribution to the overall bending stiffness. These concepts are discussed in more details in section 5.5.7.

If the sandwich beam is subjected to shear forces, it is necessary to determine the shear stress distribution over the cross-section. Proceeding along the same path as in

the previous section, the basic equation of equilibrium, eq. (15.6), is used to solve for the shear stress distribution in the lower face, to find

$$\tau_f = \frac{1}{2} E_f \left(\frac{h + t_f}{2} \right)^2 \left[\left(\frac{2x_2}{h + t_f} \right)^2 - 1 \right] \frac{\mathrm{d}^2 \Phi_3}{\mathrm{d}x_1^2}.$$

Because the axial stiffness of the core is negligible, the axial stress vanishes, and the basic equation of equilibrium, eq. (15.6), yields $\mathrm{d}\tau_{12}/\mathrm{d}x_2 = 0$. Hence, the shear stress is constant through the thickness of the core.

The shear stress must be continuous at the face/core interface implying that

$$\tau_c = \frac{1}{2} E_f \left(\frac{h + t_f}{2} \right)^2 \left[\left(\frac{h - t_f}{h + t_f} \right)^2 - 1 \right] \frac{\mathrm{d}^2 \Phi_3}{\mathrm{d}x_1^2} = -\frac{1}{2} E_f h t_f \frac{\mathrm{d}^2 \Phi_3}{\mathrm{d}x_1^2}.$$

In view of the symmetry of the problem, the shear stress in the top face is a mirror image of that in the lower face, as depicted in fig. 15.5. The shear force is then obtained by integrating this shear stress distribution over the cross-section to find

$$V_2 = -\frac{1}{2} E_f b h^2 t_f \left[1 + \frac{1}{3} \left(\frac{t_f}{h} \right)^2 \right] \frac{\mathrm{d}^2 \Phi_3}{\mathrm{d}x_1^2} \approx -\frac{1}{2} E_f b h^2 t_f \frac{\mathrm{d}^2 \Phi_3}{\mathrm{d}x_1^2}.$$

Eliminating $\mathrm{d}^2\Phi_3/\mathrm{d}x_1^2$ between the previous two equations yields the shear stress in the core in term of the applied shear force

$$\tau_c = \frac{V_2}{bh}.$$

This result indicates that the shear force is carried entirely by a uniform shear stress in the core. The shear stress in the faces contribute little to the load carrying capability of the sandwich, although the faces carry most of the bending stress, σ_1.

Finally, the strain energy associated with the shear deformation in the sandwich beam is

$$\mathrm{d}A = \frac{1}{2} \int_{\mathcal{A}} \frac{\tau_{12}^2}{G} \, \mathrm{d}\mathcal{A} \mathrm{d}x_1 = \frac{b}{2} \int_{-h/2}^{h/2} \frac{\tau_c^2}{G_c} \, \mathrm{d}x_2 \mathrm{d}x_1 = \frac{1}{2} \frac{\tau_c^2}{G_c} bh \, \mathrm{d}x_1 = \frac{1}{2} \frac{V_2^2}{bhG_c} \, \mathrm{d}x_1.$$

It follows that the shear stiffness of the sandwich is

$$K_{22} = bhG_c. \tag{15.16}$$

This analysis reveals an important aspect of the structural behavior of sandwich structures. Whereas the bending stiffness and strength of sandwich beams are inherited solely from the stiffness and strength characteristics of the faces, the shear stiffness and strength of these structures are inherited from the stiffness and strength characteristics of the core. Because the mechanical properties of the core are generally much lower than those of the faces, shear failure in the core can possibly occur for applied loads far below those that would result in failure of the faces. Consequently, the evaluation of shear stress distributions plays an important role in the analysis and design of sandwich structures.

15.1.3 Problems

Problem 15.1. Simply supported beam under uniform load
Consider a beam with a solid rectangular cross-section under shear loads. In the process of developing a theory to model the deformation of the beam based on the assumption that plane sections remain plane, the two different shear stress distributions and associated shear strain distributions have been obtained and are depicted in fig. 15.4. *(1)* Why is the simplified deformation mode an incorrect solution? *(2)* Why is the improved deformation mode an incorrect solution?

Problem 15.2. Simply supported beam under uniform load
Consider a simply supported beam of length L subjected to a uniform transverse load p_0. The beam has a rectangular section of width b and depth h and is made of a homogeneous material. *(1)* Find the magnitude and location of the maximum axial stress in the structure. Sketch the axial stress distribution for this section. *(2)* Find the magnitude and location of the maximum shear stress in the structure. Sketch the shear stress distribution for this section. *(3)* Is the mid-span deflection of the beam affected by shearing deformations? How can you assess the importance of this effect? *(4)* Is the mid-span bending moment in the beam affected by shearing deformations? How can you assess the importance of this effect? *(5)* If the beam is cantilevered at both ends, how would your answers to the last two questions change?

Problem 15.3. Cross-section made of two materials
The cross-section of a sandwich beam is depicted in fig. 15.6. The subscript $(\bullet)_c$ refers to core quantities, whereas the subscript $(\bullet)_f$ refers to facing quantities. *(1)* Determine the shear stress distribution over the cross-section. *(2)* Evaluate the corresponding shear force V_2. *(3)* Plot the shear stress distribution $\tau_{12}bh/V_2$ and compute the shearing stiffness of the section $K_{22}/(G_c bh)$. Use $h_c/h = 2/3.6$, $E_c/E_f = 70/140$, $G_c/G_f = 70/140$. *(4)* Plot the shear stress distribution $\tau_{12}bh/V_2$ and compute the shearing stiffness of the section $K_{22}/(G_c bh)$. Consider a sandwich with a soft core $E_c \approx 0$ and very thin facings $t/h \ll 1$, $t = (h - h_c)/2$.

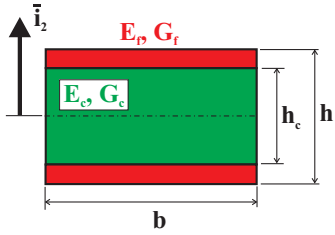

Fig. 15.6. Cross-section made of two materials.

15.2 Shear deformable beams: an energy approach

Consider the cantilevered beam subjected to distributed transverse loads, $p_2(x_1)$, distributed bending moments, $q_3(x_1)$, a concentrated tip load, P_2, and a bending moment, Q_3, as depicted in fig. 15.7. The transverse displacement is assumed to take place in plane $(\bar{\imath}_2, \bar{\imath}_1)$. The strain energy stored in the beam can be evaluated using the general expression for the strain energy in a three-dimensional solid, eq. (10.46),

$$A = \frac{1}{2}\int_0^L \int_{\mathcal{A}} \underline{\sigma}^T \underline{\epsilon}\, \mathrm{d}\mathcal{A}\mathrm{d}x_1,$$

where L is the length of the beam and $\mathcal{A}$ its cross-sectional area.

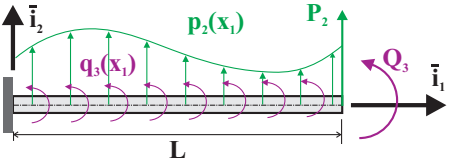

Fig. 15.7. Cantilevered beam under distributed and concentrated transverse loads and bending moments.

The kinematics are shown in fig. 15.8 where a cross-section containing point **P** is shown before and after deformation. Plane sections of the beam are assumed to remain plane, leading to an axial displacement field in the form of eq. (5.2): $u_1(x_1, x_2, x_3) = -x_2\Phi_3(x_1)$, where $\Phi_3(x_1)$ is the rotation of the section about axis $\bar{\imath}_3$ as shown in fig. 15.8. For simplicity, the centroid of the section is assumed to be located of the origin of the axis system, *i.e.*, $x_{2c} = 0$. The cross-section of the beam is also assumed to remain rigid in its own plane, leading to a transverse displacement field in the form of eq. (5.1), $u_2(x_1, x_2, x_3) = \bar{u}_2(x_1)$.

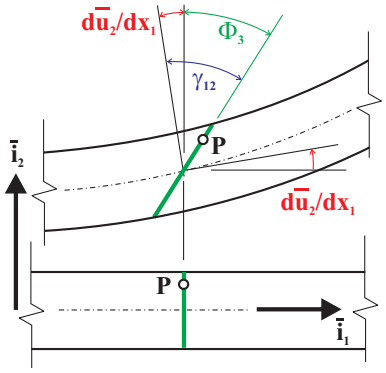

Fig. 15.8. Kinematic assumptions for shear deformable beams.

The axial strain distribution is then obtained as $\epsilon_1 = \partial\bar{u}_1/\partial x_1 = -x_2\,\mathrm{d}\Phi_3/\mathrm{d}x_1$, and the transverse shear strain is

$$\gamma_{12} = \frac{\partial u_1}{\partial x_2} + \frac{\partial u_2}{\partial x_1} = -\Phi_3 + \frac{\mathrm{d}\bar{u}_2}{\mathrm{d}x_1}. \quad (15.17)$$

In Euler-Bernoulli theory, the transverse shear strain is assumed to vanish, $\gamma_{12} = 0$, and hence the rotation of the section, Φ_3, is equal to the slope of the beam, $\mathrm{d}\bar{u}_2/\mathrm{d}x_1$. In the present development, illustrated in fig. 15.8, the shear strain given by eq. (15.17) is the difference between the slope of the beam and the rotation of its cross-section. The beam slope and sectional rotation are the independent variables of the theory.

The strain energy expression now reduces to

$$A = \frac{1}{2}\int_0^L \int_{\mathcal{A}} (\sigma_1\varepsilon_1 + \tau_{12}\gamma_{12})\ \mathrm{d}\mathcal{A}\mathrm{d}x_1.$$

The stress components, σ_2, σ_3, and τ_{23} acting in the plane of the cross-section are assumed to be much smaller than the axial stress, σ_1, and hence, Hooke's law implies $\sigma_1 = E\epsilon_1$ and $\tau_{12} = G\gamma_{12}$. Introducing these constitutive relationships and strain fields into the strain energy yields

$$A = \frac{1}{2}\int_0^L \left\{ \left[\int_{\mathcal{A}} Ex_2^2\,\mathrm{d}\mathcal{A}\right]\left(\frac{\mathrm{d}\Phi_3}{\mathrm{d}x_1}\right)^2 + \left[\int_{\mathcal{A}} G\,\mathrm{d}\mathcal{A}\right]\left(\frac{\mathrm{d}\bar{u}_2}{\mathrm{d}x_1} - \Phi_3\right)^2 \right\} \mathrm{d}x_1.$$

The term in the first square bracket is the bending stiffness of the beam, H_{33}^c, see eq. (5.36). The curvature of the beam is still $\mathrm{d}\Phi_3/\mathrm{d}x_1$, but in view of eq. (15.17) it does not equal $\mathrm{d}^2\bar{u}_2/\mathrm{d}x_1^2$ as is the case for Euler-Bernoulli beam theory. The two expressions are different now because the slope of the beam no longer equals the rotation of the section. The term in the second square bracket is the shear stiffness, and for beams made of homogeneous, linearly elastic material, this stiffness is $G\mathcal{A}$, as developed in section 15.1.1. With these results, the strain energy becomes

$$A = \frac{1}{2}\int_0^L \left[H_{33}^c \left(\frac{\mathrm{d}\Phi_3}{\mathrm{d}x_1} \right)^2 + G\mathcal{A} \left(\frac{\mathrm{d}\bar{u}_2}{\mathrm{d}x_1} - \Phi_3 \right)^2 \right] \mathrm{d}x_1.$$

At this point, the transverse shear strain is assumed to be uniformly distributed over the cross-section, see eq. (15.17). This is a direct consequence of assuming plane sections to remain plane after deformation, and therefore, the strain distribution is identical to that of the simplified representation discussed in section 15.1.1. This explains why the shear stiffness, $G\mathcal{A}$, in the present formulation is identical to that for the simplified representation.

As discussed in section 15.1.2, the simplified and equilibrium based representations can be made equivalent from an energy perspective by selecting the average shear strain to be $\gamma_{\mathrm{ave}} = V_2/K_{22}$, see eq. (15.12). With the help of eqs. (15.10) and (15.17), the shear strain energy for the equilibrium based representation is then $\mathrm{d}A = 1/2\ K_{22}\gamma_{\mathrm{ave}}^2\,\mathrm{d}x_1 = 1/2\ K_{22}(\mathrm{d}\bar{u}_2/\mathrm{d}x_1 - \Phi_3)^2$. Thus, it is only necessary to replace the shear stiffness, $G\mathcal{A}$, in the above equation by its more accurate counterpart, K_{22}, to obtain the shearing strain energy corresponding to the equilibrium based representation. Consequently, the following expression gives the strain energy stored in a beam subjected to bending and shearing

$$A = \frac{1}{2}\int_0^L \left[H_{33}^c \left(\frac{\mathrm{d}\Phi_3}{\mathrm{d}x_1} \right)^2 + K_{22} \left(\frac{\mathrm{d}\bar{u}_2}{\mathrm{d}x_1} - \Phi_3 \right)^2 \right] \mathrm{d}x_1, \tag{15.18}$$

where the first term represents the strain energy associated with bending of the beam and the second is that associated with shearing. The total potential energy of the complete beam system can now be expressed as

$$\begin{aligned} \Pi = \frac{1}{2}\int_0^L \left[H_{33}^c \left(\frac{\mathrm{d}\Phi_3}{\mathrm{d}x_1} \right)^2 + K_{22} \left(\frac{\mathrm{d}\bar{u}_2}{\mathrm{d}x_1} - \Phi_3 \right)^2 \right] \mathrm{d}x_1 \\ - \int_0^L (p_2\bar{u}_2 + q_3\Phi_3)\ \mathrm{d}x_1 - P_2\bar{u}_2(L) - Q_3\Phi_3(L). \end{aligned} \tag{15.19}$$

Given the total potential energy, the principle of minimum total potential energy can be used to derive the governing differential equations of the problem and associated boundary conditions. This principle requires the total potential energy to be stationary for all arbitrary choices of the displacement fields $\bar{u}_2(x_1)$ *and* $\Phi_3(x_1)$, leading to

$$\delta\Pi = \int_0^L \left[H_{33}^c \frac{\mathrm{d}\Phi_3}{\mathrm{d}x_1}\, \delta\left(\frac{\mathrm{d}\Phi_3}{\mathrm{d}x_1}\right) + K_{22}\left(\frac{\mathrm{d}\bar{u}_2}{\mathrm{d}x_1} - \Phi_3\right) \delta\left(\frac{\mathrm{d}\bar{u}_2}{\mathrm{d}x_1} - \Phi_3\right)\right] \mathrm{d}x_1 - \int_0^L \left(p_2\, \delta\bar{u}_2 + q_3 \delta\Phi_3\right) \mathrm{d}x_1 - P_2 \delta\bar{u}_2(L) - Q_3 \delta\Phi_3(L) = 0.$$

Integration by parts and interchanging the variational and differential operators then yields the following expression

$$\begin{aligned}\delta\Pi = &\int_0^L \delta\Phi_3 \left\{ -\frac{\mathrm{d}}{\mathrm{d}x_1}\left(H_{33}^c \frac{\mathrm{d}\Phi_3}{\mathrm{d}x_1}\right) - K_{22}\left(\frac{\mathrm{d}\bar{u}_2}{\mathrm{d}x_1} - \Phi_3\right) - q_3 \right\} \mathrm{d}x_1 \\ &+ \int_0^L \delta\bar{u}_2 \left\{ -\frac{\mathrm{d}}{\mathrm{d}x_1}\left[K_{22}\left(\frac{\mathrm{d}\bar{u}_2}{\mathrm{d}x_1} - \Phi_3\right)\right] - p_2 \right\} \mathrm{d}x_1 + \left[H_{33}^c \frac{\mathrm{d}\Phi_3}{\mathrm{d}x_1}\, \delta\Phi_3 \right]_0^L \\ &+ \left[K_{22}\left(\frac{\mathrm{d}\bar{u}_2}{\mathrm{d}x_1} - \Phi_3\right) \delta\bar{u}_2 \right]_0^L - P_2 \delta\bar{u}_2(L) - Q_3 \delta\Phi_3(L) = 0.\end{aligned} \tag{15.20}$$

This expression must vanish for all arbitrary variations $\delta\Phi_3$ and $\delta\bar{u}_2$, and therefore the two integrand terms in braces must vanish, leading to the Euler-Lagrange equations for the problem

$$\frac{\mathrm{d}}{\mathrm{d}x_1}\left(H_{33}^c \frac{\mathrm{d}\Phi_3}{\mathrm{d}x_1}\right) + K_{22}\left(\frac{\mathrm{d}\bar{u}_2}{\mathrm{d}x_1} - \Phi_3\right) = -q_3, \tag{15.21a}$$

$$\frac{\mathrm{d}}{\mathrm{d}x_1}\left[K_{22}\left(\frac{\mathrm{d}\bar{u}_2}{\mathrm{d}x_1} - \Phi_3\right)\right] = -p_2. \tag{15.21b}$$

For the cantilevered beam depicted in fig. 15.7, the geometric boundary conditions at the root of the beam are $\bar{u}_2 = 0$ and $\Phi_3 = 0$. At the tip of the beam, the variations $\delta\Phi_3(L)$ and $\delta\bar{u}_2(L)$ are arbitrary, and the boundary terms of eq. (15.20) yield the following boundary conditions

$$H_{33}^c \frac{\mathrm{d}\Phi_3}{\mathrm{d}x_1} = Q_3, \text{ and } \quad K_{22}\left(\frac{\mathrm{d}\bar{u}_2}{\mathrm{d}x_1} - \Phi_3\right) = P_2. \tag{15.22}$$

These two natural boundary conditions are readily interpreted as $M_3^c = Q_3$ and $V_2 = P_2$, which are the equilibrium equations at the loaded end of the beam.

In summary, the problem of a shear deformable beam is governed by two second order, coupled ordinary differential equations, eqs. (15.21), for the two unknown displacement fields, $\bar{u}_2(x_1)$ and $\Phi_3(x_1)$. Four boundary conditions are required to solve these equations. Once these differential equations are solved, the bending moment and shear force distributions can be recovered as $M_3^c = H_{33}^c\, \mathrm{d}\Phi_3/\mathrm{d}x_1$ and $V_2 = K_{22}\,(\mathrm{d}\bar{u}_2/\mathrm{d}x_1 - \Phi_3)$, respectively.

The governing equations, eqs. (15.21), can be rewritten in terms of stress resultants as $\mathrm{d}M_3^c/\mathrm{d}x_1 + V_2 = -q_3$, and $\mathrm{d}V_2/\mathrm{d}x_1 = -p_2$. They represent the equilibrium conditions for a differential element of the beam and are identical to those obtained for Euler-Bernoulli beam theory, see eq. (5.38). This should be expected

because equilibrium equations always apply, no matter what kinematic assumptions are made.

While the equilibrium equations are identical for Euler-Bernoulli and shear deformable beam theories, the relationships that involve kinematic quantities are different. For instance, in shear deformable beams, the bending moment-curvature relationship is $M_3^c = H_{33}^c \mathrm{d}\Phi_3/\mathrm{d}x_1$. Therefore, it would be erroneous to use the corresponding relationship from Euler-Bernoulli beam theory, *i.e.*, $M_3^c \neq H_{33}^c \, \mathrm{d}^2\bar{u}_2/\mathrm{d}x_1^2$.

Finally, eq. (15.19) for the total potential energy can also be used to obtain approximate solutions for shear deformable beam problems in a manner similar to that described in section 11.4.2 for Euler-Bernoulli beams. Both transverse displacement *and* sectional rotation fields must be approximated with the help of suitable sets of shape functions. This technique will be demonstrated in later sections.

15.2.1 Shearing effects on beam deflections

Consider the uniform, cantilevered beam of length L subjected to a concentrated transverse load P acting at a distance αL from its root, as depicted in fig. 15.9. The differential equilibrium equations for the beam are given by eqs. (15.21). For the first segment of the beam with $0 \leq x_1 \leq \alpha L$, the differential equations are

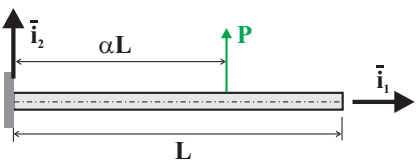

Fig. 15.9. Cantilevered beam with concentrated transverse load.

$$H_{33}^c \frac{\mathrm{d}^2\Phi_3}{\mathrm{d}x_1^2} + K_{22}\left(\frac{\mathrm{d}\bar{u}_2}{\mathrm{d}x_1} - \Phi_3\right) = 0, \quad \frac{\mathrm{d}}{\mathrm{d}x_1}\left[K_{22}\left(\frac{\mathrm{d}\bar{u}_2}{\mathrm{d}x_1} - \Phi_3\right)\right] = 0.$$

The boundary conditions at the beam's root are $\bar{u}_2 = 0$ and $\Phi_3 = 0$, and at $x_1 = \alpha L$, they are $K_{22}\,(\mathrm{d}\bar{u}_2/\mathrm{d}x_1 - \Phi_3) = P$ and $H_{33}^c \, \mathrm{d}\Phi_3/\mathrm{d}x_1 = 0$.

Integration of the second governing equation yields $K_{22}\,(\mathrm{d}\bar{u}_2/\mathrm{d}x_1 - \Phi_3) = c_1$, where c_1 is an integration constant which is determined from the boundary condition at $x_1 = \alpha L$ to be $c_1 = P$. Hence $K_{22}\,(\mathrm{d}\bar{u}_2/\mathrm{d}x_1 - \Phi_3) = P$. Because $K_{22}\,(\mathrm{d}\bar{u}_2/\mathrm{d}x_1 - \Phi_3) = K_{22}\,\gamma_{\mathrm{ave}} = V_2$, this means that $V_2 = P$, and therefore the transverse shear force is constant along the span of the beam, a result that could have been obtained from simple equilibrium considerations.

Introducing this result into the first governing equation yields $H_{33}^c \, \mathrm{d}^2\Phi_3/\mathrm{d}x_1^2 + P = 0$. With the help of the boundary conditions, this integrates to

$$\Phi_3 = \frac{PL^2}{H_{33}^c}\left(-\frac{1}{2}\eta^2 + \alpha\eta\right),$$

where $\eta = x_1/L$ is the non-dimensional variable along the span of the beam.

Finally, the transverse displacement field is found by integrating $\mathrm{d}\bar{u}_2/\mathrm{d}x_1 = \Phi_3 + P/K_{22}$ and using the boundary condition, $\Phi_3(0) = 0$, to find

$$\bar{u}_2 = \frac{PL^3}{6H_{33}^c}\left(-\eta^3 + 3\alpha\eta^2\right) + \frac{PL}{K_{22}}\eta.$$

A similar process can be followed to find the displacement field over the second segment of the beam, $\alpha L \leq x_1 \leq L$. The boundary conditions at the beam's tip are $V_2 = K_{22}\left(\mathrm{d}\bar{u}_2/\mathrm{d}x_1 - \Phi_3\right) = 0$ and $M_3^c = H_{33}^c\,\mathrm{d}\Phi_3/\mathrm{d}x_1 = 0$, whereas continuity conditions on $\bar{u}_2$ and Φ_3 are applied at $x_1 = \alpha L$.

The transverse displacement field for the complete beam becomes

$$\bar{u}_2(\eta) = \frac{PL^3}{6H_{33}^c}\begin{cases}\eta^2(3\alpha - \eta) + 6\bar{s}^2\eta, & 0 \leq \eta \leq \alpha,\\ \alpha^2(3\eta - \alpha) + 6\bar{s}^2\alpha, & \alpha \leq \eta \leq 1,\end{cases} \tag{15.23}$$

where

$$\bar{s}^2 = \frac{H_{33}^c}{K_{22}L^2} \tag{15.24}$$

is a non-dimensional *shear flexibility parameter* defining the shear flexibility relative to the bending flexibility.

The sectional rotation is

$$\Phi_3(\eta) = \frac{PL^2}{2H_{33}^c}\begin{cases}\eta\left(-\eta + 2\alpha\right), & 0 \leq \eta \leq \alpha,\\ \alpha^2, & \alpha \leq \eta \leq 1.\end{cases} \tag{15.25}$$

The non-dimensional shear flexibility parameter, $\bar{s}^2$, measures the importance of shear deformations relative to bending deformations. For an Euler-Bernoulli beam, the shear modulus is assumed to be infinite, the shear stiffness is then also infinite, and the shear flexibility parameter vanishes. Using $\bar{s}^2 = 0$ in eq. (15.23), the transverse displacement for an Euler-Bernoulli beam is recovered, see eq. (5.55).

Example 15.2. Shear deformation in a tip loaded cantilevered beam

Consider the case of a cantilevered beam with a tip load, P. The tip deflection is obtained by introducing $\alpha = 1$ and $\eta = 1$ into eq. (15.23) to find

$$\bar{u}_2(1) = \frac{PL^3}{3H_{33}^c}\left(1 + 3\bar{s}^2\right). \tag{15.26}$$

The first term represents the tip deflection due to bending, denoted δ_b, and the second is the additional contribution due to shear deformation, denoted δ_s. The ratio of these two contributions is

$$\frac{\delta_s}{\delta_b} = 3\bar{s}^2. \tag{15.27}$$

If the shear stiffness decreases, the shear flexibility parameter increases and the tip deflection due to shear deformations becomes more and more pronounced compared to that due to bending.

To relate the shear flexibility parameter to the physical characteristics of beams, the two cross-sections depicted in fig. 15.10 will be investigated. Consider first a solid

rectangular section of width b and depth h made of a linearly elastic, homogeneous material. The shear flexibility parameter is

$$\bar{s}^2 = \frac{bh^3E}{12}\,\frac{6}{5bhG}\,\frac{1}{L^2} = \frac{1}{10}\left(\frac{E}{G}\right)\left(\frac{h}{L}\right)^2. \tag{15.28}$$

The shear flexibility parameter is the product of two ratios: a material property ratio, E/G, and a geometric aspect ratio, h/L. The material property ratio is the ratio of Young's modulus to the shearing modulus. For a linearly elastic, homogeneous and isotropic material, this ratio is $E/G = 2(1+\nu)$. The geometric aspect ratio is the ratio of the depth of the beam to its length, and it is a powerful contributor to the shear flexibility parameter because the ratio is squared.

For many engineering materials such as steel, aluminum, or titanium, Poisson's ratio is about 0.3, and the shear flexibility parameter becomes solely a function of the geometric aspect ratio, $\bar{s}^2 = 0.26(h/L)^2$. For long beams, the shear flexibility parameter quickly tends to zero, and shear deformation effects quickly become negligible. It is perhaps more useful to consider the reverse reasoning. As the beam's length decreases, bending deformations decrease fast, and shear deformations to become relatively more pronounced.

Example 15.3. Shear deformation of a sandwich beam

Consider next a sandwich section such as that depicted in the left part of fig. 15.10 as "cross-section A." The bending and shearing stiffnesses are given by eqs. (15.15) and (15.16), respectively, and hence, the shear flexibility parameter becomes

$$\bar{s}^2 = \frac{tbh^2E_f}{2}\,\frac{1}{bhG_c}\,\frac{1}{L^2} = \frac{1}{2}\left(\frac{E_f}{G_c}\right)\left(\frac{t_f}{h}\right)\left(\frac{h}{L}\right)^2. \tag{15.29}$$

The shear flexibility parameter is again the product of two ratios: a material property ratio, E_f/G_c, and a geometric aspect ratio, h/L. The ratio t_f/h characterizes the relative thickness of the faces. The material property ratio is the ratio of Young's modulus of the faces, E_f, to the shearing modulus of the core, G_c. There is, of course, no intrinsic relationship between these two moduli because they are the properties of two different materials.

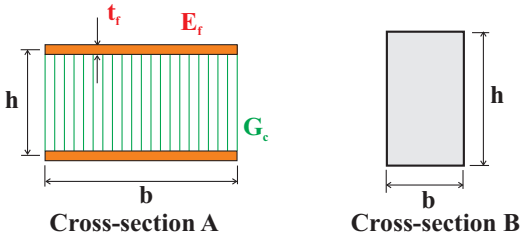

Fig. 15.10. Two different cross-sections for a beam.

Consider, for instance, a sandwich with aluminum faces ($E_f = 73$ GPa), and an aluminum honeycomb core ($G_c = 1$ GPa). The material ratio is then $E_f/G_c = 73$,

as compared to $E/G = 2.6$ for a homogeneous aluminum beam. This implies much larger shear flexibility parameters for sandwich constructions as compared solid sections made of homogeneous material. The geometric aspect ratio is the ratio of the depth of the beam to its length and its effect is similar to that discussed earlier.

To quantitatively assess the importance of shear deformations, the following two cases will be considered. The first is an aluminum beam ($E/G = 2.6$) with a rectangular cross-section shown as "cross-section B" in fig. 15.10. Two beam aspect ratios will be investigated, a long beam, $h/L = 1/10$, and a shorter beam, $h/L = 1/5$.

The second case is a sandwich beam with thin composite faces, $t_f/h = 1/10$, and an aluminum honeycomb core, $E_f/G_c = 70 \times 10^9/1 \times 10^9 = 70$, shown as "cross-section A" in fig. 15.10. Here again, both long and short beams will be considered.

Table 15.1 summarizes the results for the two cases, listing the values of the shear flexibility parameters given by eqs. (15.28) and (15.29), respectively, and the corresponding relative magnitude of the transverse displacement due to shear deformations at the tip of the beam, see eq. (15.27).

Table 15.1. Effect of shear deformation on the tip deflection of a tip-loaded cantilevered beam.

	Rectangular section		Sandwich section	
h/L	1/10	1/5	1/10	1/5
$\bar{s}^2$	2.6×10^{-3}	10.4×10^{-3}	35.0×10^{-3}	140.0×10^{-3}
$\delta_s/\delta_b(\%)$	0.78%	3.1%	10.5%	42%

For the beam with a solid rectangular section, the results indicate a rather small influence of shearing deformations. Only for very short beams do shearing effects become significant; beam theory itself, however, is valid only for structures having one dimension larger than the other two, *i.e.*, $L/h \gg 1$. Hence, shearing effects are unlikely to be very significant for such structures.

This contrasts with the case of sandwich beams. As indicated in table 15.1, much larger values of the shear flexibility parameter are found for these structures, resulting in much larger contributions of shear deformations to the total transverse displacement. With a 42% contribution to the total transverse displacement for a sandwich beam with an aspect ratio $h/L = 1/5$, shear deformations cannot be ignored. Of course, the stress resultants in the beam are identical to those obtained from Euler-Bernoulli beam theory, because stress resultants can be evaluated from equilibrium considerations alone.

Example 15.4. Cantilevered beam with intermediate support

A cantilevered beam of span L features an intermediate support at location $x_1 = \alpha L$ and is subjected to a tip load, P, as depicted in fig. 15.11. This is a hyperstatic configuration, and hence the reactions cannot be determined without considering the deformation of the beam. The force method from section 4.3.3 will be employed and both bending and shearing deflections will be included.

To begin, the intermediate support is replaced by a reaction force, R, of unspecified magnitude. The transverse displacement field under this combined loading then follows from eq. (15.23)

$$\bar{u}_2(\eta) = \frac{L^3}{6H^c_{33}} \begin{cases} R\left[\eta^2(3\alpha-\eta)+6\bar{s}^2\eta\right] + P\left[\eta^2(3-\eta)+6\bar{s}^2\eta\right], & 0 \le \eta \le \alpha, \\ R\left[\alpha^2(3\eta-\alpha)+6\bar{s}^2\alpha\right] + P\left[\eta^2(3-\eta)+6\bar{s}^2\eta\right], & \alpha \le \eta \le 1, \end{cases}$$

where $\eta = x_1/L$ is the non-dimensional variable along the beam's span.

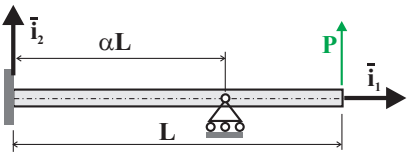

Fig. 15.11. Cantilevered beam with intermediate support.

The unknown reaction force at the support point is found by imposing the vanishing of the transverse displacement at $\eta = \alpha$. From $\bar{u}_2(\alpha) = 0$, it follows that

$$R = -\frac{\alpha(3-\alpha)+6\bar{s}^2}{2\alpha^2+6\bar{s}^2}\,P = -\mu\,P. \tag{15.30}$$

Because this problem is hyperstatic, the reaction force depends on the deformations of the system, and in this case, it depends on the magnitude of shearing deformations as is evident from the presence of the shear flexibility parameter in the above expression. Substituting for the support reaction force, R, from eq. (15.30) yields the transverse displacement in terms of the applied load

$$\bar{u}_2(\eta) = \frac{PL^3}{6H^c_{33}} \begin{cases} \left[-(1-\mu)\eta^3+3(1-\alpha\mu)\eta^2+6(1-\mu)\bar{s}^2\eta\right], & 0 \le \eta \le \alpha, \\ \left[-\eta^3+3\eta^2-3\mu\alpha^2\eta+\mu\alpha^3+6(\eta-\alpha\mu)\bar{s}^2\right], & \alpha \le \eta \le 1, \end{cases}$$

Next, the rotation of the section is found with the help of eq. (15.25)

$$\Phi_3(\eta) = \frac{L^2}{2H^c_{33}} \begin{cases} R\left(-\eta^2+2\alpha\eta\right) + P\left(-\eta^2+2\eta\right), & 0 \le \eta \le \alpha, \\ R\left(\alpha^2\right) + P\left(-\eta^2+2\eta\right), & \alpha \le \eta \le 1, \end{cases}$$

and introducing the support reaction force yields the sectional rotation in terms of the applied load

$$\Phi_3(\eta) = \frac{PL^2}{2H^c_{33}} \begin{cases} \left[-(1-\mu)\eta^2+2(1-\alpha\mu)\eta\right], & 0 \le \eta \le \alpha, \\ \left(-\eta^2+2\eta-\mu\alpha^2\right), & \alpha \le \eta \le 1. \end{cases}$$

The bending moment distribution in the beam then follows from the sectional constitutive law, $M_3 = \mathrm{d}\Phi_3/\mathrm{d}x_1$, as

$$M_3(\eta) = PL \begin{cases} [-(1-\mu)\eta + (1-\alpha\mu)], & 0 \le \eta \le \alpha, \\ (1-\eta), & \alpha \le \eta \le 1. \end{cases}$$

Finally, the shear force distribution is found from the sectional constitutive law, $V_2 = K_{22}(\mathrm{d}\bar{u}_2/\mathrm{d}x_1 - \Phi_3)$, as

$$V_2(\eta) = P \begin{cases} (1-\mu), & 0 \le \eta \le \alpha, \\ 1, & \alpha \le \eta \le 1. \end{cases}$$

Figure 15.12 shows the transverse displacement distribution and sectional rotation of the beam for $\alpha = 0.6$. The first case shown on the figure is an Euler-Bernoulli solution obtained by setting $\bar{s}^2 = 0$ in the above expressions. For the second case, a beam with an aspect ratio, $h/L = 1/10$, is assumed with a solid rectangular cross-section made of aluminum. The shear flexibility parameter, $\bar{s}^2$, given by eq. (15.28), is $\bar{s}^2 = 0.0026$. The third case features a sandwich beam with $t_f/h = 1/10$ and $E_f/G_c = 70$. The shear flexibility parameter, $\bar{s}^2$, given by eq. (15.29), is $\bar{s}^2 = 0.035$, assuming $h/L = 1/10$. Little difference is observed between the Euler-Bernoulli solution ($\bar{s}^2 = 0$) and the shear deformable solution with $\bar{s}^2 = 0.0026$. For the sandwich structures, however, the beam's tip displacement is markedly larger, 67%, as compared to Euler-Bernoulli predictions.

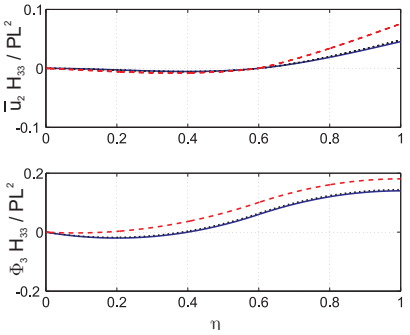

Fig. 15.12. Transverse displacement (top figure) and sectional rotation (bottom figure) of the cantilevered beam with an intermediate support, $\alpha = 0.6$. Shear flexibility parameter $\bar{s}^2 = 0$, solid line; $\bar{s}^2 = 0.0026$, dotted line; $\bar{s}^2 = 0.035$, dashed line.

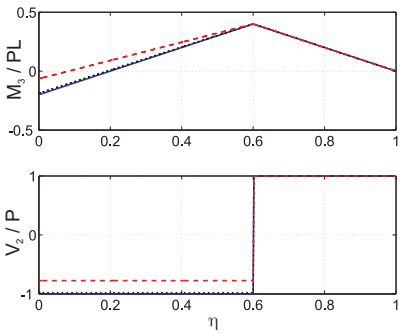

Fig. 15.13. Bending moment (top figure) and shear force (bottom figure) of the cantilevered beam with an intermediate support, $\alpha = 0.6$. Shear flexibility parameter $\bar{s}^2 = 0$, solid line; $\bar{s}^2 = 0.0026$, dotted line; $\bar{s}^2 = 0.035$, dashed line.

Figure 15.13 shows the bending moment and shear force distributions along the beam for the same three cases. Here again, little difference is observed between the Euler-Bernoulli solution ($\bar{s}^2 = 0$) and the shear deformable solution with $\bar{s}^2 = 0.0026$. For the overhanging portion of the beam, $\alpha \le \eta \le 1$, the stress resultants are readily obtained from equilibrium considerations and hence, are identical for all values of the shear flexibility parameter.

For the remaining portion of the beam, $0 \leq \eta \leq \alpha$, the stress resultants are dependent on the reaction force at the support. This reaction force is obtained from a kinematic conditions, $\bar{u}_2(\eta = \alpha) = 0$, and is a function of the deformation of the beam. Consequently, in this portion of the beam, both displacements *and* stress resultants are affected by shearing deformations.

Two features of the shear deformable solution are worth noting. First, the root slope of the beam does not vanish; indeed, at $\eta = 0$, $\mathrm{d}\bar{u}_2/\mathrm{d}x_1 = PL^2/H^c_{33}\ (1 - \mu)\bar{s}^2 = (1 - \mu)P/K_{22} = V_2/K_{22} = \gamma_{12}$. Clearly, the root shear strain does not vanish, and hence, the slope of the beam is not zero, although the sectional rotation does indeed vanish. Second, the slope of the beam is discontinuous at the intermediate support. To see this, let $\alpha^- = \alpha - \varepsilon$ and $\alpha^+ + \varepsilon$ where $\varepsilon \to 0$ denote stations of the beam just before and after the intermediate support, respectively. It is then readily found that $\mathrm{d}\bar{u}_2(\alpha^+)/\mathrm{d}x_1 - \mathrm{d}\bar{u}_2(\alpha^-)/\mathrm{d}x_1 = PL^2/H^c_{33}\ \mu\bar{s}^2 = P\mu/K_{22} = -R/K_{22}$. Clearly, the slope discontinuity is a direct consequence of the shear force discontinuity at the same location.

Example 15.5. Unit load method for beams including shear deformations

The transverse deflections of beams including shear deformations can be calculated using the unit load method developed section 9.7.6. The unit load method is a direct application of the principle of complementary virtual work and states that $\Delta\delta D + \delta W'_I = 0$, where Δ is the prescribed displacement, δD the virtual driving force, and $\delta W'_I$ the complementary internal virtual work in the beam. For an Euler-Bernoulli beam, this latter quantity is given by eq. (9.79b). To include shear deformations in the unit load method, the complementary internal virtual work done by virtual shear forces undergoing actual shear strains must also be taken into account.

For beams presenting symmetry with respect to plane $(\bar{\imath}_1, \bar{\imath}_2)$ and subjected to bending moments M_3 only, the complementary internal virtual work reduces to $\delta W'_I = -\int_0^L \kappa_3 \delta M_3 \mathrm{d}x_1$. With the addition of the complementary internal virtual work done by virtual shear forces undergoing actual shear strains, this becomes

$$\delta W'_I = -\int_0^L \left(\kappa_3 \delta M_3 + \gamma_{\mathrm{ave}} \delta V_2\right) \mathrm{d}x_1, \tag{15.31}$$

where γ_{ave} is given by eq. (15.12).

Following the reasoning developed section 9.7.6, the unit load method applied to shear deformable beams leads to the following expression for the displacement at a point of the beam

$$\Delta = \int_0^L \left(\frac{M_3 \hat{M}_3}{H^c_{33}} + \frac{V_2 \hat{V}_2}{K_{22}}\right) \mathrm{d}x_1. \tag{15.32}$$

A unit load is applied at the point and in the direction of the desired displacement component. The bending moment distribution, M_3, and shear force distribution, V_2, are those acting in the beam under the action of the externally applied loads. The bending moment distribution, $\hat{M}_3$, and shear force distribution, $\hat{V}_2$, are statically admissible bending moment and shear force distributions in equilibrium with the unit load. The displacement component, Δ, is then computed by eq. (15.32).

To illustrate the unit load method applied to shear deformable beams, consider a cantilevered beam of length L subjected to a tip load P. For this isostatic problem, the bending moment and shear force distributions are easily found from statics considerations as $M_3 = -Px_1$ and $V_2 = P$, respectively. The statically admissible bending moment and shear force distributions in equilibrium with a unit tip load are then $\hat{M}_3 = -x_1$ and $\hat{V}_2 = 1$, respectively. Equation (15.32) then yields the desired tip displacement as

$$\Delta = \int_0^L \left[\frac{(-Px_1)(-x_1)}{H_{33}^c} + \frac{(P)(1)}{K_{22}} \right] \mathrm{d}x_1 = \frac{1}{3} \frac{PL^3}{H_{33}^c} + \frac{PL}{K_{22}}.$$

Introducing the shear flexibility parameter, $\bar{s}$, defined in eq. (15.24), leads to

$$\Delta = \frac{1}{3} \frac{PL^3}{H_{33}^c} \left(1 + 3\bar{s}^2\right),$$

which agrees with eq. (15.26).

15.2.2 Shearing effects on buckling

In chapter 14, the buckling load of a simply supported beam under axial compressive loads is found using Euler-Bernoulli beam theory. If the beam is shear deformable, the additional compliance of the system will lower the buckling load, implying that the predictions based on Euler-Bernoulli theory overestimate the actual buckling load.

To investigate the effect of shear deformation on buckling loads, an energy approach will be used. Consider a uniform, simply-supported beam subjected to an end compressive load of magnitude P. The total potential energy of the system is obtained by combining the strain energy for a shear deformable beam, eq. (15.18), and the potential of the axial load, eq. (14.37), to find

$$\begin{aligned} \Pi = & \frac{1}{2} \int_0^L H_{33}^c \left(\frac{\mathrm{d}\Phi_3}{\mathrm{d}x_1} \right)^2 \mathrm{d}x_1 + \frac{1}{2} \int_0^L K_{22} \left(\frac{\mathrm{d}\bar{u}_2}{\mathrm{d}x_1} - \Phi_3 \right)^2 \mathrm{d}x_1 \\ & - \frac{1}{2} \int_0^L P \left(\frac{\mathrm{d}\bar{u}_2}{\mathrm{d}x_1} \right)^2 \mathrm{d}x_1, \end{aligned}$$

where the first term represents the strain energy associated with the bending of the beam, the second term that associated with its shearing, and the last term the work done by the axial compressive load, P.

The following displacement shape functions will be assumed

$$\bar{u}_2(x_1) = q_1 \sin \frac{\pi x_1}{L}, \quad \Phi_3(x_1) = q_2 \cos \frac{\pi x_1}{L}. \tag{15.33}$$

The mode shape assumed for the transverse displacement corresponds to the exact solution of the problem using Euler-Bernoulli theory. The mode shape assumed for

the sectional rotation is the derivative of the assumed transverse displacement. Because the sectional rotation is not equal to the slope of the beam, coefficients q_1 and q_2 are different for a shear deformable beam.

Introducing the assumed shape functions into the expression for the total potential energy and integrating over the beam span then yields

$$\Pi = \frac{1}{2}\frac{L}{2}\left[H_{33}^c\left(\frac{\pi}{L}\right)^2 q_2^2 + K_{22}\left(\left(\frac{\pi}{L}\right)^2 q_1^2 - \frac{2\pi}{L}q_1 q_2 + q_2^2\right) - P\left(\frac{\pi}{L}\right)^2 q_2^2\right].$$

This expression can be recast into a matrix format as two quadratic forms given by

$$\begin{aligned}\Pi &= \frac{1}{2}\underline{q}^T\frac{L}{2}\begin{bmatrix}\left(\frac{\pi}{L}\right)^2 K_{22} & -\frac{\pi}{L}K_{22} \\ -\frac{\pi}{L}K_{22} & \left(\frac{\pi}{L}\right)^2 H_{33}^c + K_{22}\end{bmatrix}\underline{q} - \frac{1}{2}\underline{q}^T\frac{PL}{2}\begin{bmatrix}\left(\frac{\pi}{L}\right)^2 & 0 \\ 0 & 0\end{bmatrix}\underline{q} \\ &= \frac{1}{2}\underline{q}^T\underline{\underline{K}}\,\underline{q} - \frac{1}{2}\underline{q}^T P\underline{\underline{K}}_G\underline{q},\end{aligned}$$

where $\underline{q} = \{q_1, q_2\}^T$ is the solution array, $\underline{\underline{K}}$ the stiffness matrix, and $\underline{\underline{K}}_G$ the geometric stiffness matrix. The buckling equation is now given by eq. (14.48), and the vanishing of the determinant leads to

$$\left(\frac{\pi}{L}\right)^2\left[\left(\frac{\pi}{L}\right)^2 H_{33}^c + K_{22}\right]P_{\rm cr} - \left(\frac{\pi}{L}\right)^4 K_{22}H_{33}^c = 0.$$

Solving for the buckling load yields

$$P_{\rm cr} = \frac{\pi^2 H_{33}^c/L^2}{1 + \pi^2 H_{33}^c/(K_{22}L^2)}.$$

The buckling load can be written in terms of the shear flexibility parameter defined by eq. (15.24) and the buckling load for an Euler-Bernoulli beam, $P_{\rm Euler} = \pi^2 H_{33}^c/L^2$, eq. (14.25), as

$$P_{\rm cr} = \frac{P_{\rm Euler}}{1 + \pi^2\bar{s}^2}.$$

For Euler-Bernoulli beams, $\bar{s}^2 = 0$, and $P_{\rm cr} = P_{\rm Euler}$, as expected. For shear deformable beams, $\bar{s}^2 > 0$, and the buckling load is always lower than $P_{\rm Euler}$ due to the additional flexibility of the system.

To quantify this effect, the beams with solid rectangular and sandwich sections described in section 15.2.1 will be examined again. Table 15.2 lists the ratios of the buckling loads to the Euler loads for the various cases. Shear deformation has a more pronounced effect on buckling loads than on static deflections. For the sandwich sections, the results indicate a 26% or 58% decrease in buckling load as compared to Euler-Bernoulli predictions for aspect ratios $h/L = 1/10$ and $1/5$, respectively. Clearly, the inclusion of shear deformation effects is critically important when computing the buckling loads of a system, even for long, slender sandwich beams.

Table 15.2. Effect of shear deformation on the buckling load of a simply supported beam.

	Rectangular section		Sandwich section	
h/L	1/10	1/5	1/10	1/5
$\bar{s}^2$	2.6×10^{-3}	10.4×10^{-3}	35.0×10^{-3}	140.0×10^{-3}
$P_{\mathrm{cr}}/P_{\mathrm{E}}$	0.98	0.91	0.74	0.42

15.2.3 Problems

Problem 15.4. Cantilevered beam under distributed bending moment
Consider a shear deformable, cantilevered beam subjected to a uniform, distributed bending moment $q_3(x_1) = q_0$. *(1)* Write the governing differential equations of the problem. *(2)* Write the boundary conditions of the problem. *(3)* Find the tip transverse displacement and sectional rotation distributions along the beam. *(4)* Is the tip deflection affected by shear deformations?

Problem 15.5. Four-point bending test
The four-point bending test set-up depicted in fig. 5.19 is routinely used to experimentally determine the bending stiffness of a beam. The load, P, applied by the testing machine is transmitted to the test sample through two rollers; the applied load is reacted underneath the test sample by two additional rollers. The deformation of the test sample is measured by two strain gauges, one located on top and the other on the bottom of the sample, as shown in fig. 5.19. Let ϵ_t and ϵ_b be the strain measurements at the top and bottom locations, respectively. *(1)* Using Euler-Bernoulli beam theory, describe the data reduction procedure that evaluates the test sample's bending stiffness given the measured load, P, and strain gauge readings, ϵ_t and ϵ_b. *(2)* What correction should be made to the data reduction procedure if the test sample is a shear deformable, sandwich structure.

Problem 15.6. Cantilevered beam with a uniform distributed load
Derive the governing equations and associated boundary conditions for the shear deformable cantilevered beam with uniform distributed load depicted in fig. 15.14. *(1)* Develop a solution for the bending deflection, $\bar{u}_2^b$, (assume $\bar{s}^2 = 0$). *(2)* Construct an approximate solution for the shear deformable beam. Use $\bar{u}_2^b$ as the shape function for the transverse displacement field and $\mathrm{d}\bar{u}_2^b/\mathrm{d}x_1$ as that for the rotation field. *(3)* Use the principle of minimum total potential energy to find the approximate solution. *(4)* Construct a table similar to table 15.1 and discuss the results.

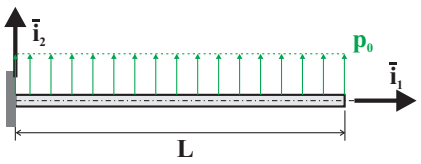

Fig. 15.14. Cantilevered beam with a uniform distributed load.

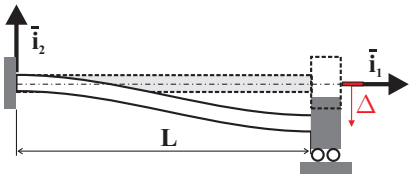

Fig. 15.15. Clamped-clamped beam with tip deflection.

Problem 15.7. Clamped-clamped beam with support misalignment
A uniform beam of length, L, is clamped at both ends, but the right hand support is misaligned by a vertical distance, Δ, as depicted in fig. 15.15. *(1)* Plot the transverse displacement field $\bar{u}_2(\eta)/\Delta$ over the span of the beam, $\eta = x_1/L$. *(2)* Plot the bending moment distribution, $L^2 M_3(\eta)/(H^c_{33}\Delta)$, over the span of the beam. *(3)* Plot the shear force distribution, $L^3 V_2(\eta)/(H^c_{33}\Delta)$, over the span of the beam. For each question, consider the following cases: *(a)* the beam has no shearing deformations (*i.e.*, assume Euler-Bernoulli beam theory); *(b)* the beam is made of steel and has a rectangular cross-section with $E/G = 2.6$ and $h/L = 1/5$, see section A in fig. 15.10; *(c)* the beam has a sandwich cross-section with $E_f/G_c = 35$, $t/h = 1/10$, $h/L = 1/5$, see section B in fig. 15.10. Parameter $\bar{s}^2 = H^c_{33}/(K_{22}L^2)$ can be used to characterize the shearing deformations. For each of the three questions, plot the results for the three cases on on a single graph.

Problem 15.8. Measuring sectional shear stiffness
Figure 15.16 depicts the experimental set-up for the four-point and three-point bending tests. The four-point bending test is discussed in example 5.3. In the four-point bending test, the test section is subjected to bending only, and in the three-point bending test, the test section is subjected to combined bending and shearing. Assume that the test sample is of sandwich construction with the configuration shown in fig. 15.10. The beam shear stiffness is denoted K_{22}. *(1)* Compute the deflection of point **M**, denoted Δ_4, for the four-point bending test. *(2)* Compute the deflection of point **M**, denoted Δ_3, for the three-point bending test. *(3)* Use these results to develop an expression for the shear stiffness, K_{22}, in term of the deflections, Δ_4 and Δ_3, and the beam properties. *(4)* Using a simple first order analysis, determine the sensitivity of this expression to errors in the measurement of Δ_4 and Δ_3. This can be done by constructing a first order Taylor's series expansion for K_{22} in terms of Δ_4 and Δ_3. Comment on your results.

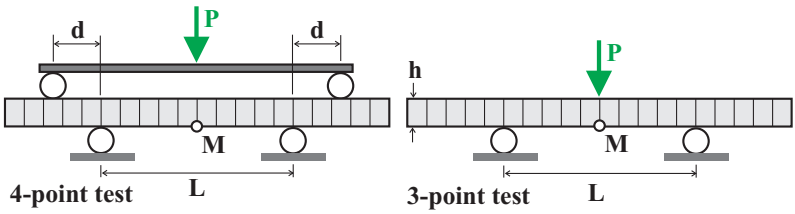

Fig. 15.16. Beam under 4-point and 3-point loading.

Problem 15.9. Cantilevered beam with tip rotational spring
Consider a cantilevered beam of length, L, with a tip rotational spring of stiffness, k, depicted in fig. 15.17. The beam is subjected to an end compressive load, P. Use an energy method to compute the buckling load of the system. The effects of shearing deformations should be included in your analysis. Assume the following displacement modes: $\bar{u}_2 = a\ (1 - \cos \pi x_1/2L)$, $\Phi_3 = b\ \sin \pi x_1/2L$. The following notation will be convenient to use: $P_{\rm E} = \pi^2 H^c_{33}/(4L^2)$, $\bar{s}^2 = \pi^2 H^c_{33}/(4K_{22}L^2)$, $\bar{k} = 8kL/(\pi^2 H^c_{33}$, where $P_{\rm euler}$ is the buckling load of the system without the tip spring and ignoring shearing deformations, $\bar{s}^2$ is the shearing deformation parameter, and k^* is the non-dimensional stiffness of the torsional spring.

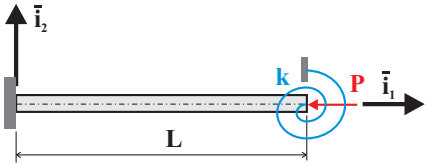

Fig. 15.17. Cantilevered beam with tip torsional spring.

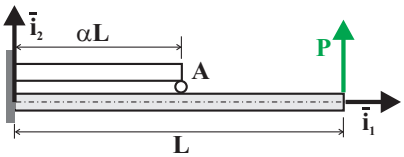

Fig. 15.18. Cantilevered beam with intermediate support.

Problem 15.10. Simply supported beam on an elastic foundation

Consider a simply supported beam of length L resting on an elastic foundation of stiffness constant k, as shown in fig. 15.19. The beam is subjected to an axial compressive force, P. Shearing deformations should be taken into account. Use an energy approach with the following assumed modes: $\bar{u}_2 = \sum_{n=1}^{\infty} U_n \sin n\pi x_1/L$; $\Phi_3 = \sum_{n=1}^{\infty} \Phi_n \cos n\pi x_1/L$. The following notation will be convenient to use: $\bar{s}^2 = \pi^2 H^c_{33}/(K_{22}L^2)$, $\bar{k} = kL^4/(\pi^4 H^c_{33})$. *(1)* Find the buckling load of the system as a function $\bar{k}$. *(2)* For a value of $\bar{k} = 12.0 \times 10^3$, find the buckling mode shape n and the buckling load of the system P/P_{euler} when shearing deformations are neglected. *(3)* Same questions when shearing deformation are taken into account. Use a beam of rectangular cross-section with $h/L = 1/10$ and $E/G = 2.6$. *(4)* Same questions for a beam of rectangular cross-section with $h/L = 1/10$ and $E/G = 28$. Note: In section 14.3, this problem is treated under the assumption of negligible shearing deformations.

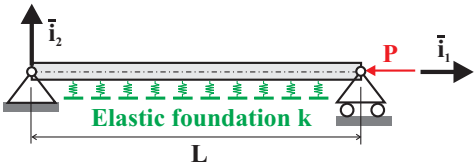

Fig. 15.19. Simply supported beam on an elastic foundation.

Problem 15.11. Cantilevered beam with intermediate support

The cantilevered beam depicted in fig. 15.18 is subjected to a tip load P. The tip of a second cantilevered beam contacts the first at point **A**. The lower and upper beams have a uniform bending stiffness, H^c_{33}, uniform shearing stiffnesses, K_{22}, and are of length L and αL, respectively. *(1)* Find the displacement fields for the two beams. *(2)* On one graph, plot the distribution of non-dimensional transverse displacement, $H^c_{33}\bar{u}_2/(PL^3)$, for both beams. *(3)* Plot the distribution of non-dimensional rotation, $H^c_{33}\Phi_3/(PL^2)$, for both beams. *(4)* Plot the distribution of non-dimensional bending moment, $M_3/(PL)$, for both beams. *(5)* Plot the distribution of non-dimensional transverse shear force, V_2/P, for both beams. Use $\alpha = 0.25$. *(6)* Study the behavior of the system as $\alpha \to 0$. *(7)* Plot the non- dimensional force in the intermediate support, F/P, as a function of $\alpha \in [0, 0.5]$. *(8)* Plot the distribution of non-dimensional transverse tip displacement, $H^c_{33}\bar{u}_2/(PL^3)$, as a function of $\alpha \in [0, 0.5]$. *(9)* Plot the distribution of non-dimensional root bending moment, $M_3/(PL)$, as a function of $\alpha \in [0, 0.5]$ for both beams. *(10)* Plot the distribution of non-dimensional root shear force, V_2/P, as a function of $\alpha \in [0, 0.5]$ for both beams. Comment on your results. For each question, consider the following three cases: *(a)* the beam has no shearing deformations (*i.e.*,

assume Euler-Bernoulli beam theory); *(b)* the beam is made of steel and has a rectangular cross-section with $E/G = 2.6$ and $h/L = 1/5$, see section A in fig. 15.10; *(c)* the beam has a sandwich cross-section with $E_f/G_c = 35$, $t/h = 1/10$, $h/L = 1/5$, see section B in fig. 15.10.